Probing adsorption sites in a cubic II water clathrate cage by methyl group rotation of CH_3I guest molecules

2004 J. Phys.: Condens. Matter 16 7045

(http://iopscience.iop.org/0953-8984/16/39/037)

INSTITUTE OF PHYSICS PUBLISHING JOURNAL OF PHYSICS: CONDENSED MATTER

J. Phys.: Condens. Matter **16** (2004) 7045–7061 PII: S0953-8984(04)75913-5

Probing adsorption sites in a cubic II water clathrate cage by methyl group rotation of CH_3I guest molecules

M Prager[1], J Pieper[2], A Buchsteiner[2] and A Desmedt[3]

[1] Institut für Festkörperforschung, Forschungzzentrum Jülich, D-52425 Jülich, Germany
[2] Hahn-Meitner Institut, Glienickerstrasse 100, D-14109 Berlin, Germany
[3] Laboratoire de Physico-Chimie Moléculaire, Université de Bordeaux I, 351 Cours de la Libération, F-33405 Talence, France

Received 5 February 2004
Published 17 September 2004
Online at stacks.iop.org/JPhysCM/16/7045
doi:10.1088/0953-8984/16/39/037

Abstract

Methyl iodide enclosed in the $5^{12}6^4$ cage of cubic II water clathrate is investigated by neutron spectroscopy in the temperature regime from 1.8 to 145 K. The three tunnelling bands observed at the lowest temperature at 497, 372 and 243 μeV of relative intensities 2 : 3 : 5 represent three distinct adsorption sites of CH_3I. Sites of occurrence probabilities corresponding closely to the observed line intensities are related to the three types of hydrogen bonds of the cage. The band at 372 μeV shows fast spin conversion compared to the two others. The corresponding site is facing the shortest O–H..O hydrogen bond with the fastest proton dynamics. Spin conversion may thus reflect hydrogen jumps within the H-bond network of host molecules. Jump rates of the order of 10^{-4} s^{-1} can be estimated. Above a temperature $T \sim 45$ K the methyl dynamics become classical and can be described by rotational diffusion on a circle. A second quasielastic process becomes visible at a higher temperature and is identified as head-to-tail flips of the whole molecule with a characteristic jump distance of about 5 Å. Above $T \sim 90$ K translational freedom of the CH_3I leads to a rattling mode appearing at $\sim$0.95 meV.

(Some figures in this article are in colour only in the electronic version.)

1. Introduction

Many simple molecules can be encaged in framework structures. An almost inert environment is offered by rare gases [1]. Matrix spectroscopy uses this technique to study individual isolated molecules and reactive radicals. The statistical distribution of guest molecules requires very low guest concentrations to avoid the effects of guest–guest interactions. With a few exceptions, the low density of scattering centres makes the application of neutron spectroscopy in this field difficult [2]. A further problem presents the locally varying environment resulting from

the non-equilibrium production procedure of the material. This leads to an inhomogeneously broadened spectral response.

A higher concentration of guest molecules not involving a deterioration of measured spectra could be obtained if a matrix with only identical environments would be available. Such systems may be offered by nature and by supramolecular chemists in the form of inclusion compounds [3, 4]. A huge variety of inclusion compounds is found by combining different host and guest molecules. Among the many possible host materials, water forms are an especially interesting and fascinating class of clathrates [4]. Their presence and importance in nature has been detected recently. Large amounts of methane clathrates are formed in the ocean shelves and the permafrost area and may represent one of the largest energy reservoirs on earth [5]. The material became widely known as 'burning ice'. Methane hydrates are also present on planets and moons in our solar system and invoke interest in the phase behaviour under the respective environmental conditions of pressure and temperature [6]. The dynamics of methane in this natural clathrate show fundamentally interesting behaviour. The large size of the cages allows for very anharmonic soft translation (rattling) and almost free rotation. Thus, at the lowest temperature, the molecule behaves as an almost free quantum rotor whose characteristic transition energies can be quantitatively described from intermolecular interaction potentials [7, 8].

Artificial water clathrates can be prepared with a wide variety of guest molecules. This versatility may also allow the incorporation of biologically interesting substances for which the ordered water cage may be considered as a model hydration shell [9]. The information on the guest–host interaction in water clathrates may thus contribute to an understanding of special aspects of living matter.

The crystal structures of water clathrates can be understood on the basis of hydrogen-bonded plane rings of water molecules. Due to the H–O..H bond angle of 109° a pentagonal arrangement of $5H_2O$ is most stable. By linking these motifs to each other via common edges, a pentagon-dodecaeder is formed. With its surface of 12 pentagons it represents one of the platonic solids and is labelled in the language of clathrate physics by the symbol 5^{12}. Since only three out of the four coordination axes of oxygen are contained in the cage surface, the fourth one is available to form the three-dimensional crystal. Energetically less favourable rings of water molecules as hexagons or squares may also be formed if larger cages are used to accommodate larger guest molecules. The cages built up by 12 pentagons and 2 or 4 hexagons are named $5^{12}6^2$ and $5^{12}6^4$, respectively. The $5^{12}6^4$ polyhedron (figure 1) contains the four hexagons in the geometry of a tetrahedron separated by pentagons. The polyhedra can be arranged to space filling regular lattices. In general, cages of different sizes are present in one structure. For example eight $5^{12}6^4$ units and sixteen 5^{12} units form the unit cell of the cubic II structure [10]. The structure determination has shown that the hydrogens occupy the two possible sites in each O–H..O bond with equal probabilities [10–12]. There are cases where only one type of cages is occupied by the guest, but often—like in the case of methane clathrate—different cages are occupied with different probabilities. Then the materials are often referred to as non-stoichiometric.

The conditions at which stable phases of clathrates are formed depend on the properties of the guest molecules. Water soluble guests like tetrahydrofuran form clathrates just by cooling the stoichiometric mixture of liquids below the new melting temperature. Methane clathrates are only stable in a certain pressure–temperature regime. This is why they exist in the ocean shelf at a depth of about 600 m and at water temperatures below 8 °C. Methyl iodide, on the other hand, is insoluble in water. To overcome the hydrophobicity of CH_3I a special preparation technique was developed [13]. The system crystallizes in the cubic II structure and stoichiometry $CH_3I{\cdot}17H_2O$. Only the $5^{12}6^4$ cages are large enough to house a methyl iodide

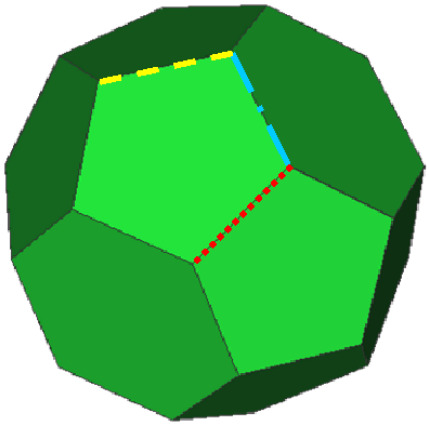

Figure 1. The large $5^{12}6^4$ cage of the methyl iodide clathrate $CH_3I{\cdot}17H_2O$, which contains the CH_3I guest molecule. Each corner represents an oxygen of the water shell, and each edge a hydrogen bond. The three inequivalent edges are marked: the dotted line connects two hexagons, the dashed-dotted line connects two pentagons and the dashed line is a cross connection. See the text.

molecule. Thus all guest molecules have geometrically identical environments. In the ideal structure, all large cages are filled by guest molecules.

Due to its simplicity and molecular symmetry, methane is the prototype three-dimensional rotor. Its first non-zero electrical multipole moment is the octupole moment. Thus, the neutral methane molecule in the water cage represents the model system of a non-polar guest. The inclusion into the two different cages of the cubic I structure, likely varying orientations of the guest molecules and the incomplete order of the host lattice, e.g. by the disorder in the hydrogen bond, lead to an adsorption potential with an inhomogeneous width. The intensity distribution can be quantitatively described by molecular dynamics calculations [7].

CH_3I is another interesting probe of the clathrate cages compared to methane. It interacts with the host surface via electrical dipole–dipole interaction. From the two types of cages of the cubic II structure, only the large ones are occupied by guest molecules. This leads to a better defined problem. Finally, the mathematical description of a one-dimensional rotor is much simpler. With these properties methyl iodide clathrate is expected to show clear and new information on water-cage surfaces.

2. Single particle rotation

The model of single-particle rotation [14] is applied to describe the data. It represents a mean-field approach. The environment of the molecule is represented by a rotational potential $V(\varphi)$. Due to the symmetry of the methyl group, $V(\varphi)$ is expressed in the form of a Fourier expansion of threefold symmetry up to order N

$$V(\varphi) = \sum_{n=1}^{N} \frac{V_{3n}}{2}(1 - \cos(3n\varphi - \varphi_{3n})). \tag{1}$$

This potential determines the excitations of the hindered rotor by the eigenvalues E_i of the stationary single particle Schrödinger equation

$$\left\{-B\frac{\partial^2}{\partial\varphi^2} + V(\varphi)\right\}\Psi_i = E_i\Psi_i. \tag{2}$$

Here $B = \hbar^2/2\Theta = 0.655$ meV is the rotational constant of the methyl group with the moment of inertia Θ. Some of the calculated eigenvalues, especially the tunnel splittings of the groundstate $\hbar\omega_t = E_1 - E_0$ can only be observed at low temperature when fluctuating terms to the potential have died out. If more transitions $E_j - E_i$ are known, the shape of the potential can be better determined.

High-resolution neutron spectroscopy is the best established technique to observe low-lying transition energies of the hindered rotor. The groundstate tunnel splitting $\hbar\omega_t$ gives rise to a simple scattering function [14, 15]

$$S(Q,\omega) = (\tfrac{5}{3} + \tfrac{4}{3} j_0(Qd))\delta(\omega) + (\tfrac{2}{3} - \tfrac{2}{3} j_0(Qd))\{\delta(\omega + \omega_t) + (\delta(\omega - \omega_t)\}. \tag{3}$$

The scattering geometry enters via the momentum transfer Q. The Q-dependent weight factor of the elastic term is called the elastic incoherent structure factor (EISF) and contains the characteristic distance d of the protons within the methyl group.

Interaction of a rotor with a phonon bath at finite temperature introduces a time-dependent fluctuating potential into the low temperature Hamiltonian equation (2). As a result of interaction with phonons, the tunnel lines shift and broaden with increasing temperature according to Arrhenius functions [16]

$$\Delta\hbar\omega_t \sim \exp\left(-\frac{E_S}{kT}\right), \qquad \Gamma_t = \Gamma_0 \exp\left(-\frac{E_\Gamma}{kT}\right). \tag{4}$$

The activation energy of line broadening is determined by resonant coupling to phonons with an energy equal to the librational energy E_{01} of the unperturbed rotor and thus $E_\Gamma = E_{01}$. On the other hand, the activation energy E_S for the shift represents an average lattice energy and leads only to limited information with respect to single-particle rotation.

At high temperatures, the methyl reorientational motion becomes classical. In the neutron scattering function, the reorientational jumps in a rotational potential of finite amplitude are represented by a quasielastic Lorentzian $L(\Gamma,\omega)$ with the linewidth Γ independent of momentum transfer Q [17]

$$S(Q,\omega) = (1 + 2j_0(Qd))\delta(\omega) + 2(1 - j_0(Qd))L(\Gamma,\omega),$$

$$L(\Gamma,\omega) = \frac{1}{\pi}\frac{\Gamma}{\Gamma^2 + \omega^2}, \qquad \Gamma(T) = \Gamma_0 \exp(-E_a/kT). \tag{5}$$

Here the jump distance d is again the proton–proton distance of the methyl group and E_a represents the activation energy of the rotational potential (1). A qualitatively similar scattering function describes reorientations of the whole molecule [17]. Due to larger jump distances, the corresponding quasielastic incoherent scattering factor $2(1 - j_0)$ is maximum at lower momentum transfers Q.

For a weak or negligible barrier height, the methyl dynamics are described as rotational diffusion on a circle of radius $\rho = d/\sqrt{3}$. This motion involves displacements of any distance. Therefore the scattering function contains an infinite number of Lorentzians [14, 17, 18]

$$S(Q,\omega) = A_0(Q\rho))\delta(\omega) + \sum_{n=1}^{\infty} A_n(Q\rho)L(\Gamma_n,\omega),$$

$$\Gamma_n(T) = n^2 D_R, \qquad D_R \sim kT \tag{6}$$

with the rotational diffusion constant D_R. For more quantitative information see [17].

3. Experiments and results

3.1. Sample preparation and characterization

Samples were prepared according to [13]. A stoichiometric mixture of one methyl iodide and 17 water molecules was stirred for some days close to its freezing point. In the case of the H_2O matrix, this temperature was about $T = +4\,^{\circ}C$. The formation of the clathrate is controlled by the transformation into a transition gel state. The melting point changes with deuteration and the preparation temperatures have to be adapted accordingly. All possible combinations of protonated and deuterated molecules, $CH_3I{\cdot}17H_2O$, $CH_3I{\cdot}17D_2O$, $CD_3I{\cdot}17H_2O$ and $CD_3I{\cdot}17D_2O$, were prepared in quantities of up to about 30 g. This way, the various isotope effects can be studied. A comparison of spectra of protonated and deuterated samples allows one to distinguish the dynamics of host and guest molecules. The materials are abbreviated in the following as HH, HD, DH and DD.

To test whether the clathrate formation was successful, neutron diffraction patterns were recorded for the two samples with deuterated host lattices using the diffractometer SV7 [19] at the research reactor FRJ2 of Forschungszentrum Jülich at a wavelength $\lambda = 1.09590$ Å. Cold polycrystalline powder was filled into a pre-cooled vanadium can of 5 mm diameter and thereafter cold-transferred into the top loader Orange cryostat of the diffractometer. Diffractograms were obtained at various sample temperatures between 6 and 200 K. All observed Bragg lines could be assigned to a cubic II unit cell of the water clathrates. Figure 2 shows the HD data as an example. For the HD and DD samples and a temperature of $T = 6$ K, lattice parameters $a = 17.067$ and 17.106 Å, respectively, are found. The lattice parameter for the HD sample increases to $a = 17.159$ Å at $T = 200$ K. Due to the presence of larger crystallites, no quantitative fit of the intensities was attempted.

The inelastic scattering experiment at the high resolution time-of-flight spectrometer NEAT at HMI, Berlin, allowed an evaluation of the elastic intensities with largely improved Q-resolution. Figure 3 shows well-defined Bragg lines in the accessible regime of momentum transfers. They are fully consistent with the low-resolution diffractogram of SV7. Since the time between these two experiments was more than two months, we learn that even long storage in the refrigerator at $-20\,^{\circ}C$ does not deteriorate the samples. The appearance of a new weak 111 peak may be due to preferential orientation by the presence of large crystallites.

3.2. Methyl rotational tunnelling

A test experiment with the fully protonated HH material at a sample temperature $T_S = 2.2$ K using the thermal neutron time-of-flight (TOF) spectrometer SV29 [20] at Forschungszentrum Jülich FZJ at a wavelength $\lambda = 3.52$ Å and energy resolution $\delta E = 0.35$ meV showed unresolved wings of the elastic line. They are an indication of large tunnel splittings of the methyl groups of the CH_3I guest molecules. The spectra presented in this work were measured with a much better energy resolution of 50 μeV at the cold TOF instrument NEAT [21] of the HMI, Berlin, using a wavelength of $\lambda = 7$ Å.

The essential information from the low temperature spectrum of a quantum rotor is the ground state tunnel splitting. In the presence of inequivalent rotors, correspondingly more splittings may be observed. The measured spectra (figure 4) show a broad distribution of tunnelling intensity with internal structure. Most surprisingly, the energy loss and gain sides show very different shapes. Explaining an assymmetry beyond a Boltzmann population factor has to take into account the metastability of the excited tunnelling state due to its different total spin $S_E = \frac{1}{2}$ compared to $S_A = \frac{3}{2}$ of the A groundstate [14]. Therefore, cooling can bring the sample into a state far from thermal equilibrium.

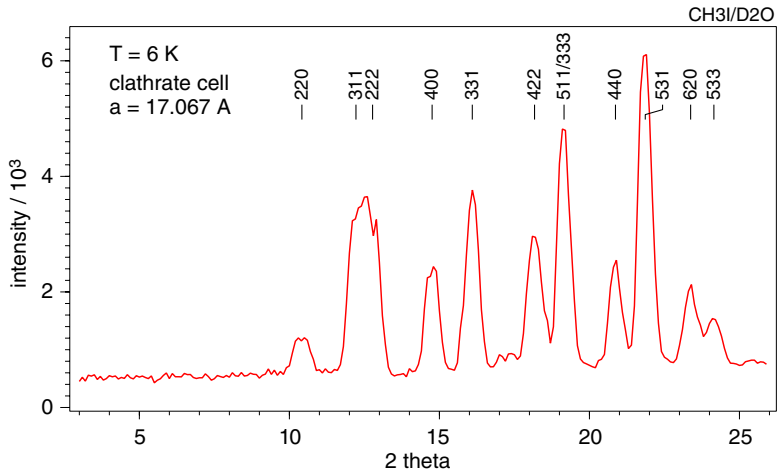

Figure 2. Diffraction pattern of methyl iodide clathrate $CH_3I{\cdot}17D_2O$. Sample temperature $T_S = 6$ K. The Bragg peaks are labelled by their Miller indices. Instrument: SV7 at FRJ2 of Forschungszentrum Jülich, $\lambda = 1.09590$ Å. The scattering angle is given in units of degrees.

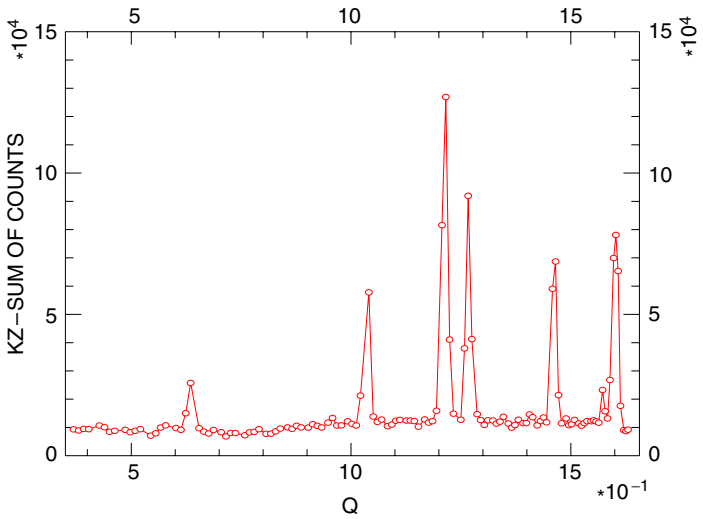

Figure 3. Diffraction pattern from methyl iodide clathrate $CH_3I{\cdot}17D_2O$. Sample temperature $T_S = 1.8$ K. Instrument: NEAT at HMI, Berlin, $\lambda = 7.0$ Å. The momentum transfer Q is given in units of Å $^{-1}$.

A first sequence of measurements was devoted to the time evolution of the nonequilibrium spectra at constant low sample temperatures. The strongest deviation from equilibrium is obtained by quenching the sample. For this purpose the HH and the HD samples were cooled from $T = 28$ to 1.8 K within 10 min. A faster cooling was not possible with the Maxi Orange cryostat used at the NEAT spectrometer. Thereafter, the evolution of the spectrum at constant temperature of the sample was registered for 12 h with a time resolution of 1 h. Figure 4 shows

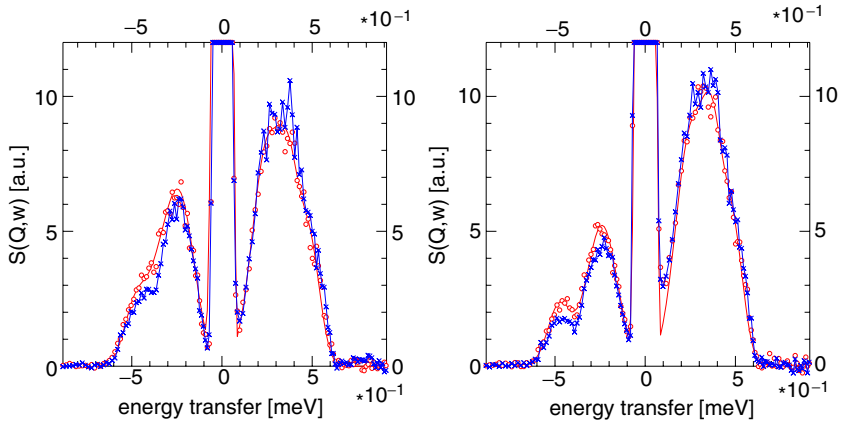

Figure 4. Spectra of methyl iodide clathrate $CH_3I{\cdot}17D_2O$ (left) and $CH_3I{\cdot}17H_2O$ (right). ○, 1 h after reaching the sample temperature $T_S = 1.8$ K; ×, after 11 h (HD) and 5 h (HH), respectively. Instrument: NEAT at HMI. $\lambda = 7.0$ Å, $\delta E_{res} = 50\ \mu$eV, $Q \sim 1.6$ Å^{-1}. The smooth solid lines are fits of the spectra at the beginning of each experiment.

on the right-hand side, the spectrum of the HH sample at the beginning of data acquisition and 11 h later. On the left-hand side, similar data for the HD sample are shown. There is a strong asymmetry of shapes at the energy loss compared to the energy gain sides. This asymmetry of the spectra is less pronounced for the HD sample. A clear doublet is seen at negative energy transfers with maxima at 497 and 243 μeV. If this doublet is mirorred to positive energy transfers and subtracted with an appropriate weight factor, a third component appears at an intermediate energy of 372 μeV.

Due to overlapping bands, the parameters of an unrestricted fit are strongly correlated. To extract reliable positions, widths and intensities we proceed in the following way. The positions and—importantly—the widths of the inner and outer tunnelling bands are taken from a fit of the energy loss side of the HH spectrum where they are well defined. The widths increase with decreasing tunnel splitting. We interpolate the width of the central tunnelling line and fix in a second step the known two positions and all line widths. Parameters of the final description are then only the position of the central tunnelling band and the six tunnelling intensities at energy loss and energy gain sides (table 1). The tunnel energies $\hbar\omega_t$ of all three inequivalent methyl species are close to the rotational constant of the methyl group $B = 0.655$ meV and thus characteristic of weak rotational potentials.

The relative intensities at energy loss and gain sides can be described by a Boltzmann factor

$$\frac{I_-}{I_+} = \exp\left(-\frac{\hbar\omega_t}{kT_{spin}}\right). \tag{7}$$

Since the excited tunnel states are not in thermal equilibrium with the lattice the spin temperature T_{spin} is in general higher than the sample temperature. Table 1 shows these spin temperatures at the beginning (t_1) and end ($t_1 + \Delta t$) of a run. While the spin temperature is close to the lattice temperature for the intermediate tunnel system it is far off from thermal equilibrium for the two extreme bands. With time the excited states become depopulated. The

Table 1. Tunnel splittings $\hbar\omega_t$ and linewidths Γ_t (half-width at half-maximum) of the tunnel bands observed. Intensities represent the sum of up- and down-scattering and are normalized to a total sum of 1. The spin temperature $T_{spin}(t)$ is obtained from equation (7). Its time evolution can be converted into a spin conversion time t_{conv}. $\Delta t = 5$ h for HH and 11 h for HD.

				$T_{spin}(t)$ (K)		
Sample	$\hbar\omega_t$ (μeV)	Γ_t (μeV)	Intensity	t_1	$t_1+\Delta t$	$t_{conv}(T_S)$ (h)
				Sample temperature $T_S = 1.8$ K		
HH	497	65	0.20	10.9	6.3	12
	372	80	0.28	1.8	1.8	$\ll$1
	243	90	0.52	6.8	4.6	26
				Sample temperature $T_S = 1.8$ K		
HD	500	65	0.16	14.5	12.1	130
	372	80	0.31	5.1	3.1	15
	242	90	0.53	14.1	10.2	110
				Sample temperature $T_S = 4.0$ K		
	500	65	0.16	17.0	5.4	9
	372	80	0.30	6.6	4.1	1
	242	90	0.53	13.0	6.4	10

spin conversion time t_{conv} describes the transition into equilibrium (*equ.* in (8)) via

$$\frac{I_-}{I_+}(t) = \exp\left(-\frac{t}{t_{conv}}\right)\left(\frac{I_-}{I_+}(0) - \frac{I_-}{I_+}(equ.)\right) + \frac{I_-}{I_+}(equ.). \tag{8}$$

For the HD and a sample temperature $T_S = 1.8$ K the intensity reduction after 12 h is of the order of 20%. The corresponding spin conversion times of the sites with the strongest and weakest rotational potential are of the order of 60–110 h while the one related with $\hbar\omega_t \sim 0.37$ meV is so short that it almost cannot be resolved within our time unit of 1 h measuring time for one spectrum. On increasing the temperature of the HD sample to $T_S = 4$ K the long spin conversion times decrease by about an order of magnitude and are now in the range of 10 h and close to those which the HH sample showed at $T_S = 1.8$ K (table 1).

The Q-dependence of the tunnelling intensities should follow the structure factor of equation (3). However, the data analysis shows that the inelastic intensity of low angle detectors saturates at a finite value for both, the HH and HD, samples. This deviation from equation (3) can only be due to multiple scattering. The presence of multiple scattering will be kept in mind when discussing classical reorientational dynamics in section 3.3.

A second sequence of measurements was devoted to the temperature evolution of the tunnelling spectrum of the HD sample until the spectral response looked quasielastic at $T \sim 40$ K. On increasing the sample temperature the excited tunnel levels become populated and the spectrum becomes more symmetric. At the same time, the tunnelling bands broaden due to coupling to phonons. Both effects hide the fine structure seen at the lowest temperatures. An average tunnelling frequency with an average width is used to model the spectra in this temperature regime. Results are shown on the left-hand side of table 2.

3.3. Classical dynamics

Above $T = 45$ K the tunnelling bands seem fully transformed into quasielastic scattering. Already at temperatures $T \sim 60$ K, the description requires two Lorentzians due to the

Table 2. Temperature dependence of an average tunnel splitting and its linewidth for temperatures $T \leqslant 30$ K and the broadening Γ_i, $i = 1, 2$ of the two quasielastic components at $T \geqslant 45$ K.

T (K)	$\hbar\omega_t$ (meV)	Γ_t (meV)	T (K)	Γ_1 (meV)	Γ_2 (meV)
14	0.286	0.140	45	0.73	0.05
17	0.279	0.164	60	0.80	0.08
20	0.271	0.193	70	1.00	0.12
25	0.26	0.25	80	1.00	0.14
28	0.24	0.30	100	1.05	0.14
30	0.21	0.33	115	1.21	0.235
			130	1.35	0.295
			150	1.48	0.345

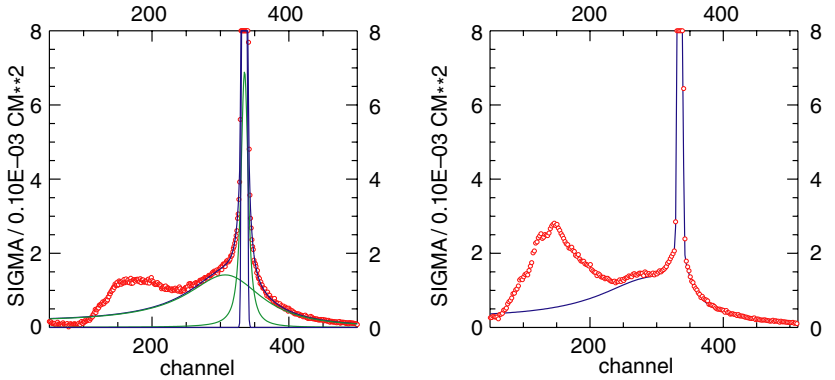

Figure 5. Effects of quasielastic and inelastic scattering are best seen in the time scale. Two quasielastic components (—) can be clearly distinguished at $T = 60$ K (left). At $T = 90$ K (right) the onset of the rattling motion (excess intensity around channel 260) is clearly visible. The maxima below channel 100 correspond to the bands of the vibrational phonon density of states at 6 and 10 meV better seen in figure 7.

appearance of a second narrower component which can be observed up to $T = 145$ K. By presenting the spectra on the time scale (figure 5), the coexisting features are more clearly distinguishable with the naked eye.

The fit regime is limited to energy transfers below 0.8 meV since higher energy transfers are strongly affected by phonon scattering. The responses of the fit parameters to changes of the selected energy range are used to estimate the systematic errors which determine the error bars in figure 6. Model-free fits show that the linewidths of both Lorentzians are independent of momentum transfer in the accessible Q-range. The linewidth of the broad Lorentzian fits well into an extrapolation of the width of the tunnelling bands (figure 6). At the same time the intensity is similar to that of the tunnelling bands. Finally, the intensity increases continuously with momentum transfer. Due to multiple scattering (see section 3.2) there is finite intensity at small momentum transfers.

While the intensity of the broad quasielastic component increases continuously with increasing momentum transfer within the accessible Q-range, that of the narrow component decreases relative to the broad component beginning at around $Q = (1.2 \pm 0.1)\,\text{Å}^{-1}$. As required, the sum of elastic and quasielastic intensities is independent of momentum transfer.

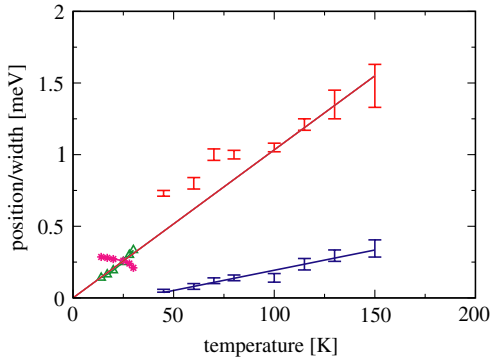

Figure 6. Evolution of the average tunnel splitting (⋆), the width of tunnelling band (△) and the linewidths of stochastic rotational motion (error bars) with temperature. Errors are systematic. The lines are guides to the eye.

There is a discontinuity in the spectra around $T \sim 90$ K. At this discontinuity the relative intensities of the two QNS components change. The narrow component becomes weaker by almost a factor 2. At the same time a low energy inelastic mode appears in the spectrum at $E_r \sim 0.95$ meV (figure 5, right-hand side, channel ∼260). This new mode gets more pronounced with further increase in temperature. It overlaps with the broadened quasielastic lines. Therefore at higher temperatures the spectra are no longer fitted but the model was adjusted to the data by hand.

3.4. Vibrational phonon density of states

Excitations in the regime of lattice modes were measured using the thermal TOF spectrometer SV29 [20] at the research reactor FRJ2 at Forschungszentrum Jülich FZJ. At a wavelength of $\lambda = 1.76$ Å the energy regime up to 20 meV is accessible with an energy resolution of $\delta E = 2.1$ meV. The temperatures of all samples were close to 2.3 K. The measured intensity is corrected for background and detector efficiencies. The generalized vibrational phonon density of states VDOS $G(\omega)$ is extracted from the scattering function

$$S(Q,\omega) = \bar{\sigma}\frac{\hbar^2 Q^2}{2\bar{m}}\exp(-2W)\frac{G(\omega)}{\hbar\omega}[n(\omega)+1] \tag{9}$$

with the mean scattering cross section $\bar{\sigma}$, the Debye–Waller factor W and the Boltzmann factor $n(\omega) + 1$. $G(\omega)$ of the HD sample is shown in figure 7. Compared to ice-h with a single strong peak at ∼6 meV the presented and all other clathrate spectra show a new band at the high-energy side of this peak. In the protonated material this peak is most pronounced, in the deuterated material it appears as a clear shoulder. The characteristic phonon energies are shown in table 3. The maxima at about 7 and 10 meV represent transverse acoustic phonons and are a fingerprint of the open cage structure of the clathrates [12, 23, 24]. A comparison with a recent study focused on the differences in the densities of states of various gas clathrates [25] shows that the present case is very similar to that of Xe or Ar water clathrates. Due to the higher energy of the primary neutrons and determination of the spectrum in energy loss of the neutrons, new details of the VDOS are seen at 14, 16, 19 and 27 meV not accessible to [25]. A comparison with the Ar clathrate in the regime up to 12 meV shows higher intensity for the high-energy band. From the scattering cross sections one calculates that, in the case of the HD

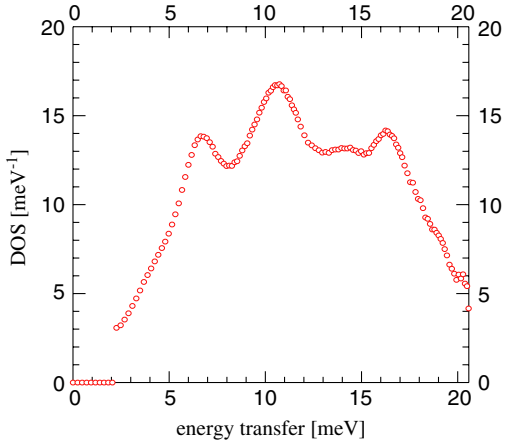

Figure 7. Generalized density of states of $CH_3I{\cdot}17D_2O$ in the meV range. Spectrometer: SV29 at FZJ, $\lambda = 1.76$ Å. Sample temperature $T = 2.3$ K.

Table 3. Maxima in the measured phonon spectra of various isotopically labelled compounds of methyl iodide clathrates and pure water H_2O. Spectrometer SV29, FZJ. Two diffraction orders with $\lambda = 1.76$ and 1.17 Å were used.

Sample	Energy transfer (meV)					
HH		6.5	10.2	17.4	20	27
DH		6.6	9.2	17		
HD	4.3	6.4	10.2	16.2		28
DD		6.2	9.6	16.6	20	27
H_2O		7.0	12.4		18	27
Assign.	CH3-lib.		External		Internal	

sample, guest and host molecules contribute to the scattering with about equal intensities. The HH or DD samples, on the other hand, are dominated by the scattering of the host lattice. This allows us to assign the lowest mode at ∼4.3 meV to a large amplitude motion of protons, the methyl libration. This observation is consistent with the finding that modes characteristic of guest molecules in gas hydrates show very low energies [23, 25, 26]. Spectra from the cubic I (Xe) and the cubic II structure (Ar, N_2, O_2) show mainly weak differences in intensities. Thus it seems impossible to distinguish clathrate structures by their VDOS measured with the energy resolution of a thermal TOF spectrometer.

4. Discussion

4.1. Adsorption sites

The prediction of the NMR experiment [13] that the methyl iodide guest in the water clathrate rotates almost freely is confirmed by our neutron scattering spectra. While NMR could not quantify the level of hindering, this is clearly possible from the measured tunnel splittings (see below section 4.2). A huge step beyond the NMR result is the observation of fine structure. The tunnelling spectrum is represented by a superposition of three lines. While

Table 4. Number N and the corresponding probability p_N of H-bonds of length d_{O-O} connecting faces of types f1 and f2 according to [11]. For direct comparison, the intensities I_{tun} of tunnelling bands of the HD sample are reproduced from table 1 together with the transition energies $\hbar\omega_t$ and spin conversion times t_{conv}.

f1	f2	N	p_N	d_{O-O}	I_{tun}	$\hbar\omega_t$	t_{conv}
5	5	24	0.57	2.796	0.52	243	26
5	6	12	0.29	2.776	0.28	372	$\ll$1
6	6	6	0.14	2.812	0.20	497	12

in the case of three-dimensional rotors like methane, symmetry reduction can split the T-states and lead to new transitions [14], the groundstate of an uncoupled, one-dimensional, threefold rotor is a doublet with a single tunnelling transition. Thus the number of tunnelling lines observed enumerates the number of inequivalent species and their intensities represent the respective occurrence probabilities. Since guest molecules occupy only the large $5^{12}6^4$ cages, the number of tunnelling transitions can only be attributed to different adsorption sites in the cages.

The relative orientations of the fullerene C_{60} in the solid phase is determined by differences in the electron density along the surface [27]. Similar inhomogeneities can be suggested to characterize the surface of the $5^{12}6^4$ clathrate cage. The most straightforward hypothesis assumes that the three crystallographically inequivalent oxygens [11] are the source of the three inequivalent adsorption sites. This model can be excluded since the surface of the $5^{12}6^4$ cage contains only two types of oxygen atoms. In addition, these two species exist with probabilities very different from the intensities of the tunnelling bands. Only four oxygens represent a contact point of three pentagons while 24 oxygens link one hexagon and two pentagons (see figure 1). By similar arguments, the two types of faces, pentagons and hexagons, can be excluded as causes of the inequivalency. The next topological element to consider are the edges. The edges represent H-bonds linking every two water molecules. There is a total of 42 edges in a cage as required by the Euler relation. Twelve edges connect a hexagon with a pentagon, 24 edges link two pentagons and six edges link two hexagons. These *three nonequivalent types of hydrogen bonds* are supposed to represent the adsorption sites. If the proposed assignment is correct, the intensities of the tunnelling lines must reflect the occurrence probablilities p_N of the adsorption sites. The hydrogen bonds are distinguished by p_N and d_{O-O} (table 4). Keeping in mind the uncertainties due to overlapping and broad lines and the related correlations between the fitted parameters, the values of table 1 show very satisfying agreement. An additional argument in favour of our assignment is based on the spin conversion and will be discussed in section 4.3. Finally, the search for other properties of the cage with three different realizations of the right occurrence probabilities as alternative explanations was not successful.

Contrary to the original expectation, each individual tunnelling band is significantly broadened. Even though all guest molecules are enclosed in identical cages, there is disorder present. The observed inhomogeneous line broadening reflects a variation in the heights of rotational barriers of about 20% within a subsite (table 5). As in methane clathrate [7], this inhomogeneous broadening is due to the multitude of possible O–H..O bond arrangements in a cage. The crystal structure determination shows that the protons in the H-bond cannot be localized [11, 12]. They all find equal population of the two possible hydrogen sites. This means that the network of hydrogen bonds of the cages varies locally and/or with time. The binding energy in methyl iodide water clathrate is dominated by the dipole–dipole interaction

Table 5. Tunnelling energies $\hbar\omega_t$, derived rotational potentials V_3 and widths ΔV_3 (half-width at half-maximum) of the related potential distribution and higher excited levels of the average potentials V_3.

$\hbar\omega_t$ (μeV)	V_3 (meV)	ΔV_3 (meV)	Calculated higher levels (meV)
497	3.6	0.9	3.2, 6.1, 6.4, 10.8
372	5.4	1.3	3.7, 6.4, 6.9, 11.2
243	8.0	2.4	4.6, 6.8, 8.0, 12.0

$U_{12}^{dip} = \vec{d}_1\vec{d}_2/r_{12}^3$. Here $|\vec{d}_1| = 1.62D$ may represent the dipole moment of methyl iodide. $\vec{d}_2$ may represent the value $1.87D$ of a water molecule. The orientation of the water dipole $\vec{d}_2$ is determined by the positions of the protons in the H-bonds. Each realization of the cage with different proton positions in the bonds is connected with a different dipolar field. The change of dipole–dipole interactions modifies both the orientation of the symmetry axis of the guest molecule and the barrier height of the weak methyl rotational potential, and thus leads to the inhomogeneous broadening of the tunnel transitions. Thus, the broadening of the tunnelling bands and the split hydrogen atoms of the diffraction experiment are two aspects of the same property.

The observed disorder could also be due to imperfect clathrate structure with local defects. Deviations from the ideal stoichiometry was indeed found for many systems. The very good agreement of the diffraction pattern with that expected for the cubic II structure and the reproducible intensities of tunnelling lines in the two different samples studied, HD and HH, makes us believe that the disorder is inherent to the cage structure and not due to imperfect samples.

4.2. Rotational potentials

Parameters of the rotational potentials are obtained by using the model of single-particle rotation of tunnelling. Assuming the simplest potential, a pure $\cos(3\varphi)$ barrier according to equation (1), the bands at 497, 372 and 243 μeV are due to potentials of heights V_3 between 3.6 and 8.0 meV (table 5). The inherent widths of the tunnelling bands can be translated into an inhomogeneous width ΔV_3 of a potential distribution [28] and amounts to about 25% of the barrier height (table 5). The calculated excited states of the CH_3 rotors (table 5) show that the band at 4.3 meV (table 3) most likely represents the first excited methyl librational level. This is confirmed by the observation that the band is only found in the VDOS of the HD sample which emphasizes the features of the guest molecules. Vice versa the energy of this band supports a $\cos(3\varphi)$ shape of the rotational potential.

The isotope effect is a sensitive test of a theoretical model. For the $\cos(3\varphi)$ potentials derived for the protonated molecules, tunnel splittings of deuterated guests of 142, 78, 35 μeV are calculated. Although the intensity of the inelastic features was weak and lines were not well resolved, it was found to be in the expected regime of transition energies. This successful scaling allows the exclusion of more complex multidimensional tunnelling models as translation–rotation coupling [29].

A quantitative interpretation of the tunnelling spectra has to be based on the crystal structure and intermolecular interaction potentials using a Monte Carlo technique. The available diffraction patterns do not allow the extraction of the required precise positions of the methyl iodide molecules. In the case of methane clathrates this information was available and such a

data analysis yielded a very satisfying almost quantitative description [7]. Methyl iodide as a one-dimensional rotor could be analysed with a simpler theoretical formalism [30].

4.3. Spin conversion

Since phonons carry no spin and since the spin is a conserved quantity, conversion processes are rare and slow. It was mainly the transformation of the energy-loss side of the tunnelling spectrum into a doublet while retaining a broad, more homogeneous, band at the energy-gain side (figure 4) which gave the strongest proof of the presence of the three adsorption sites discussed above. Spin conversion times t_{conv} are obviously not universal constants but—similar to the rotational potentials—a property of the adsorption sites. The theory shows that a necessary condition of spin conversion is a mixing of methyl quantum rotor states of different nuclear spins. Magnetic dipolar coupling [31, 32] of the methyl protons is the dominant mechanism to do this mixing. The corresponding matrix elements are proportional to d^{-3} with d being the distance between the interacting spins. Secondly, there must be a process to remove the energy connected with the $E \rightarrow A$ tunnelling transition. The responsible mechanism is rotor–phonon coupling. Since the product of phonon (x) and angular φ displacement enters this interaction [31], for example by a term $x \cdot \cos 3\varphi$, the large amplitude H-bond motion in hydrogen-bonded systems may dominate the coupling to the lattice. Based on this theory the fast spin conversion time of the methyl group, related with the tunnel splitting of 372 μeV must be due either to especially strong magnetic interaction or to more efficient rotor–phonon coupling. Since the dominant dipolar coupling mechanism is internal between the protons of the rotating methyl group, the dipolar matrix elements are determined by the same distance $d_{\mathrm{H-H}}$ of the methyl group and are thus similar for all methyl groups [31]. Small differences in the geometry of the three adsorption sites cannot play a role. The different conversion times must thus be due to different coupling strengths to the host phonons. Based on the intensities of the tunnelling bands (table 4) the fast converting methyl species related with $\hbar\omega_t = 372$ μeV faces the shortest hydrogen bond of the cage with the fastest tunnelling rate. The methyl spin conversion seems to reflect these dynamics. The intensities of the tunnelling bands at 243 μeV and 497 μeV facing longer hydrogen bonds of the cage decrease more slowly and with almost equal conversion times.

The anomalous high mobility of protons in water was proposed by the Dutch chemist de Grotthuss [33] to be 'structural diffusion'. Later the mechanism behind this word was identified as the tunnelling process in hydrogen bonds. In the meantime, quantum chemical *ab initio* calculations have shown [34] that these dynamics are much more complex than originally thought. It was found that the presence and migration of defects play important roles. The most important defect of a water structure is the hydronium ion H_3O^+, which always coexists with a hydroxyl group. Such defects are mobile with a rate τ_H^{-1} and responsible for the conductivity of the material. If we consider the coupling to the hydronium migration as the important rotor–phonon interaction there are two scenarios. The methyl conversion follows each change of the environment, and then we observe directly the proton tunnelling in the water network via the spin conversion of the methyl group. In this case, $\tau_H = \tau_{conv}$. Table 1 shows that $\tau_{conv} \sim 10^4$ s at $T = 2.3$ K. However, the recently demonstrated complexity of a H-bond tunnelling process [34] shows that there are already dynamics—and therewith coupled to it is the spin conversion—present even if there is finally no transition into the new equilibrium H-bond position. In this case, the estimated spin conversion time τ_{conv} is faster than the H-bond tunnelling and represents an upper limit of the proton delocalization time.

The temperature dependence of spin conversion times (table 1) agrees with this theory [31, 32] and earlier experiments [35]. The lower the sample temperature the smaller the number

of phonons and the slower the spin conversion. The number of temperatures studied with our system is too small to identify a specific coupling process.

4.4. Temperature effects

Three temperature regimes can be distinguished.

4.4.1. Tunnelling regime. The increasing population of the excited tunnelling state with rising temperature and the line broadening by coupling to phonons makes the three tunnelling sublines merge. Above a sample temperature of $T \sim 14$ K the subbands can no longer be distinguished. Therefore, the quantitative description of coupling tunnelling rotors to phonons (equation (4)) is based on a single Lorentzian which only characterizes an average species. The Lorentzian broadens almost linearly with temperature in contrast to the case of strong potentials where an Arrhenius-type behaviour is calculated [16] and found for almost all investigated systems. This linear broadening with temperature is interpreted as the precursor of the rotational diffusion found in the classical regime (see below).

The shift can be described by an Arrhenius-type behaviour with an activation energy of $E_a = 5.2$ meV and a prefactor of 0.4 meV. This prefactor is consistent with earlier studied tunnelling systems. The activation energy is close to the energy of the excited rotational level of the most strongly hindered methyl species (table 3). Thus, this characteristic energy seems to be dominated by the majority species.

4.4.2. Methyl rotational diffusion. The Q-independent linewidth characterizes the motion as rotation [17]; the similarity of the intensity of the broad quasielastic component with that of the tunnel bands is attributed to methyl groups. The low rotational barrier related to the observed large tunnel splittings makes methyl rotational diffusion the most likely dynamical process at higher temperature. The scattering function of rotational diffusion is an infinite sum of Lorentzians of increasing linewidths. Since the higher-order terms contribute at larger momentum transfers only, the present experiment with its limited Q-range cannot distinguish rotational diffusion from jump reorientation via the momentum transfer dependence of the quasielastic linewidth [36]. Therefore, the temperature dependence of the linewidth is analysed. While in strong potentials this width is due to reorientational jumps which obey an Arrhenius law, it is given by a rotational diffusion constant D_{rot} for negligible barrier. According to the Einstein relation, $D_{rot} = kT/\zeta_0\Theta_D$ increases linearly with temperature. The friction constant ζ_0 is defined by a Langevin equation. Θ_D is the Debye temperature. This behaviour is clearly observed in figure 6. The slope $\mathrm{d}\Gamma/\mathrm{d}T$ is the same as observed for the broadening of the tunnelling lines. Deviations in the regime $40 \leqslant T\ (\mathrm{K}) \leqslant 80$ reflect the influence of tunnelling in this temperature range: the reduced but finite offset of the broad tunnel band leads to an additional *apparent broadening* if the spectrum is fitted by a single quasielastic Lorentzian. (In the case of methane clathrate with the factor 2 larger tunnel splitting of a three-dimensional almost-free rotor, the tunnel bands can clearly be identified up to temperatures $T \sim 77$ K [8].) The smooth continuation of broadening of the tunnelling band into the width of the quasielastic line further confirms the identification of this process as methyl rotational diffusion.

The continuous increase of the quasielastic intensity with momentum transfer shows that the jump distance related with this component is rather short and consistent with the carbon–proton distance of the methyl group. An independent confirmation by the Q-dependence would have required a larger range of momentum transfers but also a thinner sample to avoid multiple scattering.

Again, our description averages over the different adsorption sites.

4.4.3. High temperature processes. Quasielastic scattering in cage structures may not only be due to methyl rotational motion but also to rotations of the whole molecule or translations in the cage. Since the second quasielastic component shows constant linewidth at all momentum transfers it is assigned to another rotational motion. A significant decrease in intensity relative to the component due to methyl group rotation is observed at around $Q_{max} = (1.2 \pm 0.1)$ Å^{-1}. The relation $Q_{max} = 2\pi/d_2$ connects this characteristic momemtum transfer with a jump distance of $d_2 \sim (5 \pm 0.5)$ Å. d_2 corresponds to about twice the carbon iodide distance $d_{C-I} =$ 2.13 Å of methyl iodide. Thus the proton–proton jump distance is about twice the size of the CH_3I molecule and fits well with 180° flips around the molecular centre of mass.

The discontinuity of the evolution of the quasielastic linewidths and intensities around 90 K must be related to a change in the molecular dynamics. We suppose that at this temperature the thermal energy kT equals the binding energy of the guest molecule and the molecule starts tumbling through the whole cage being repelled from the opposite side. Such rattling motions show low energies due to shallow adsorption potentials. The new inelastic mode at 0.95 meV appearing at $T = 90$ K is assigned to such a rattling mode in analogy to similar modes seen in the cubic I clathrates of xenon [7] and other gases [26]. Due to coupling to 180° flips the intensity of the rattling mode may be taken from the corresponding quasielastic line and thus explain the intensity reduction of the narrower quasielastic Lorentzian at 90 K.

5. Conclusion

Methyl iodide water clathrate crystallizes in the cubic II structure with space group Fd3m. The adsorption of methyl iodide on the inner surface of the $5^{12}6^4$ water cages is determined by dipole–dipole interaction of the polar guest and host molecules. The potential surface is studied by inelastic neutron scattering via rotational tunnelling of the methyl group and by quasielastic scattering at higher temperatures. The three tunnelling bands observed are assigned to three adsorption sites related to the three inequivalent hydrogen bonds of the water cage. The intensities of the tunnel bands fit reasonably well to the occurence probabilities of the three H-bonds. The rotational potentials related with these sites are weak with barriers lower than 8 meV. Equal distribution of the water protons onto the two possible sites in a hydrogen bond leads to disorder and a corresponding distribution of rotational potentials in each subsite. This disorder is the origin of the ∼20% inhomogeneous broadening of the tunnelling lines. The three adsorption sites differ strongly with respect to their spin conversion times. Rotor–phonon coupling dominated by the large amplitude tunnelling motion in the H-bond of the water cage associated with an adsorption site is proposed to cause the observed spin conversion. In agreement with this idea the shortest conversion times are found for guest molecules facing the shortest hydrogen bond of the cage.

The classical dynamics of the methyl iodide guest molecules show a complex sequence of motions. With an increase in temperature, tunnelling rotation of the methyl groups transforms into classical rotational diffusion on a circle. At $T \sim 60$ K the molecule begins to reorient by head-to-tail flips. Around the temperature $T \sim 90$ K the thermal energy begins to exceed the weak binding energy. The new translational freedom manifests itself by the appearance of a rattling mode at the low energy of 0.95 meV.

The data illustrate the astonishing complexity of a water shell. They prove that the dynamics of small molecules can be a unique probe of such potential surfaces. Similar potentials may determine the interaction of biological compounds with hydration shells.

The presented phenomonological data analysis shall be complemented by model calculations on the basis of pair interaction potentials as soon as a full structure of the methyl iodide clathrate is available.

Acknowledgments

We thank Dr J Allgaier from FZJ for the preparation of the samples and Dr W Schäfer and R Skowronek, Institut für Mineralogie, University of Bonn, for confirming the formation of the clathrate by establishing the crystal structures of our materials.

References

[1] Cradock S and Hinchcliffe A J 1975 *Matrix Isolation* (Cambridge: Cambridge University Press)
[2] Langel W, Schuller W, Knözinger E, Fleger H-W and Lauter H-J 1988 *J. Chem. Phys.* **89** 1741
[3] Atwood J L, Davies J E D and MacNicol D D (ed) 1991 *Inclusion Compounds* vol 5 (Oxford: Oxford University Press)
[4] Vögtle F 1992 *Supramolekulare Chemie* (Stuttgart: Teubner)
[5] Kvenvolden K A 1993 *Rev. Geophys.* **31** 173
[6] Loveday J S, Nelmes R J, Guthrie M, Belmonte S A, Allan D R, Klug D D, Tse J S and Handa Y P 2001 *Nature* **410** 661
[7] Gutt C, Press W, Hüller A, Tse J and Casalta H 2001 *J. Chem. Phys.* **114** 4160
[8] Tse J S, Ratcliffe C I, Powell B M, Sears V F and Handa Y P 1997 *J. Phys. Chem.* **101** 4491
[9] Nakasako M 2002 *J. Biol. Phys.* **28** 129
[10] Sloan E D Jr 1990 *Clathrate Hydrates of Natural Gases* (New York: Marcel Dekker)
[11] Hollander F and Jeffrey G A 1977 *J. Chem. Phys.* **66** 4699
[12] Gutt C, Asmussen B, Press W, Johnson M R, Handa Y P and Tse J 2000 *J. Chem. Phys.* **113** 4713
[13] Albayrak C 1988 Dissertation, Aachen
[14] Press W 1981 *Single Particle Rotations in Molecular Crystals, Springer Tracts in Modern Physics* vol 81 (Berlin: Springer)
[15] Prager M and Heidemann A 1997 *Chem. Rev.* **97** 2933
[16] Hewson A C 1982 *J. Phys. C: Solid State Phys.* **15** 3841 and 3855
[17] Bée M 1988 *Quasielastic Neutron Scattering* (Bristol: Adam Hilger)
[18] Sears V F 1966 *Can. J. Phys.* **44** 1999
Sears V F 1967 *Can. J. Phys.* **45** 234
[19] http://www.fz-juelich.de/iff/Institute/ins/Broschuere_NSE/sv7.shtml
[20] Prager M 2000 *Physica* **283** 376
http://www.fz-juelich.de/iff/Institute/ins/Broschuere_NSE/sv29.shtml
[21] Lechner R E, Melzer R and Fitter J 1996 *Physica* B **226** 86
[22] Asmussen B, Press W, Prager M and Blank H 1993 *J. Chem. Phys.* **98** 158
[23] Chazallon B, Itoh H, Koza M, Kuhs W F and Schober H 2002 *Phys. Chem. Chem. Phys.* **4** 4809
[24] Baumert J, Gutt C, Shpakov V P, Tse J S, Krisch M, Müller M, Requardt H, Klug D D, Janssen S and Press W 2003 *Phys. Rev.* B **68** 174301
[25] Schober H, Itoh H, Klapproth A, Chihaia V and Kuhs W F 2003 *Eur. Phys. J.* E **12** 41
[26] Chazallon B and Kuhs W F 2002 *J. Chem. Phys.* **117** 308
[27] David W I F, Ibberson R M, Matthewman J C, Prassides K, Dennis T J, Hare J P, Kroto H W, Taylor R and Walton D R M 1991 *Nature* **254** 408
[28] Colmenero J, Mukhopadhyay R, Alegria A and Frick B 1998 *Phys. Rev. Lett.* **80** 2350
[29] Havighorst M, Prager M and Coddens G 1996 *Chem. Phys. Lett.* **259** 1
[30] Prager M, Schiebel P and Combet J 2002 *Chem. Phys.* **276** 69
[31] Würger A 1990 *Z. Phys.* B **81** 273
[32] Häusler W 1990 *Z. Phys.* B **81** 265
[33] de Grotthuss C J T 1806 *Ann. Chim.* **LVIII** 54
[34] Marx D, Tuckerman M E, Hutter J and Parrinello M 1999 *Nature* **397** 601
[35] Grieger S, Friedrich H, Guckelsberger K, Scherm R and Press W 1998 *J. Chem. Phys.* **109** 3161
[36] Eckert J and Press W 1978 *J. Chem. Phys.* **68** 4465